Supporting Information

In Situ Measuring Partition Coefficient at Intact Nanoemulsions: A New Application of Single Entity Electrochemistry

Hiranya Madawala[1], Shashika Gunathilaka Gunathilaka Sabaragamuwe[1], Subhashini Elangovan[1], Jiyeon Kim[1]*

[1.] Department of Chemistry, University of Rhode Island, Kingston, RI, 02881

*To whom correspondence should be addressed.

Phone: +1 (401) 874-2143. E-mail: jkim25@uri.edu.

Table of Contents

1. Experimental Section

Synthesis of Nanoemulsions. NEs are prepared as reported elsewhere. [S1] Briefly, 1.8 mg of KTFPB and 250.0 mg of F127 were dissolved in 3.0 mL of THF in the vial (Fisher Scientific, 8 DR) to form a homogeneous solution. Then, 8.8 μL of DOS was added to this solution. This THF cocktail was mixed for 1 hour using a vortex mixer (Fisher Scientific, Pittsburgh, PA) at a spinning speed of 3000 rpm. After mixing, a 0.1 mL aliquot from this mixed THF cocktail was forcefully injected into 4.0 mL of nanopure water in the vial (Fisher Scientific, 4 DR) during vortex mixing at a spinning speed of 4000 rpm, and then continuously vortex mixed for 2 min. This process was immediately repeated for another batch. The resulting 8 mL of nanopure water containing the THF cocktail was then combined and homogenized (Kinematica AG, Polytron system PT 10-35 GT, Switzerland) for 2 min at a rate of 4900 rpm. In this case, 8 mL is the minimum volume used to suppress froth formation during homogenization (with a 4 DR vial). After homogenization, the meniscus level of the resulting mixture was marked. Then, the solution was further purged with N_2 gas to fully evaporate THF for 1 hour under a flow rate of 40 psi. Finally, the meniscus level of solution was marked again. A volume reduction of roughly ~1 mL was observed after the evaporation step with resulting total ~7 mL aqueous solution, which is a NE stock solution. Based on the original DOS volume of 85.7 nL in the NE stock solution and the volume of a single NE with 20~23 nm radius, i.e. ~45 zL, we could estimate the concentration of NE stock solution as ~450 pM.

Measuring the Size and Zeta potential of Nanoemulsions. NEs were characterized by carrying out the dynamic light scattering (DLS) experiment to measure the size, size distribution and ζ-potential using Zetasizer instrument (Malvern Zetasizer Nano ZS, Malvern Instruments Inc., MA). Measurements were taken at 90◦ angle for the NEs. For the DLS sample preparation, 1.0 mL of NE stock solution was diluted with 3.0 mL of nanopure water, and a 1.0 mL aliquot of this diluted solution was taken to fill a DLS cuvette (Malvern DTS 1070, Malvern Instruments Inc., MA). DLS measurements were obtained using a Malvern Nano ZS at 25 °C.

Fabrication of Pt ultramicroelectrodes (Pt UMEs). Pt UME (5 μm diameter) was fabricated using the model P-2000 (Sutter Instrument) CO_2- Laser capillary Puller. 25 μm dia. Pt wire (Goodfellow, annealed) was inserted in the borosilicate capillary (I.D. 0.2 mm, O.D. 1mm, item No 9-000-2000, Drummond scientific company, Broomall, PA) and was pulled together with CO_2 laser puller. As-pulled Pt UME was milled by a homemade polisher to expose Pt disk

resulting in an inlaid disk-shaped electrode. Then, the Pt UME was cleaned in piranha solution for 30s. The prepared Pt UME was also used under 30 % or higher relative humidity at 22~23 °C.

TEM measurements with Uranyless negative staining method. The NEs were visualized with TEM (JEM-2100F, JEOL, MA) at 100 kV. First, specimens were prepared by depositing 3.0 µL of NE suspension on the carbon side of a 300 mesh Cu TEM grid with C/Formvar film (FCF-300, Electron Microscopy Sciences, Hatfield, PA) (NE suspension: 1.0 ml of NE stock sample was diluted with 3.0 ml of nanopure water). After 30 s of NE deposition step, remaining solvent was wicked with filter paper. Then, immediately the grid was immersed in a drop of Uranyless negative stain (Delta Microscopies, France) for 30 s. Uranyless negative stain offers a better contrast on the organic molecules by staining non-radioactive lanthanide mix. The excess stain was wicked using filter paper, and the grid was dried overnight at room temperature and ambient pressure prior to imaging.

2. Characterization of NEs by Dynamic Light Scattering (DLS)

The synthesized NEs are characterized by DLS showing average diameter of 38 nm with polydisperse index 0.15, and zeta potential –15 mV. Notably, after rigorous mixing with vortex followed by 2 hr sitting on the benchtop, NEs retained the same properties without aggregation.

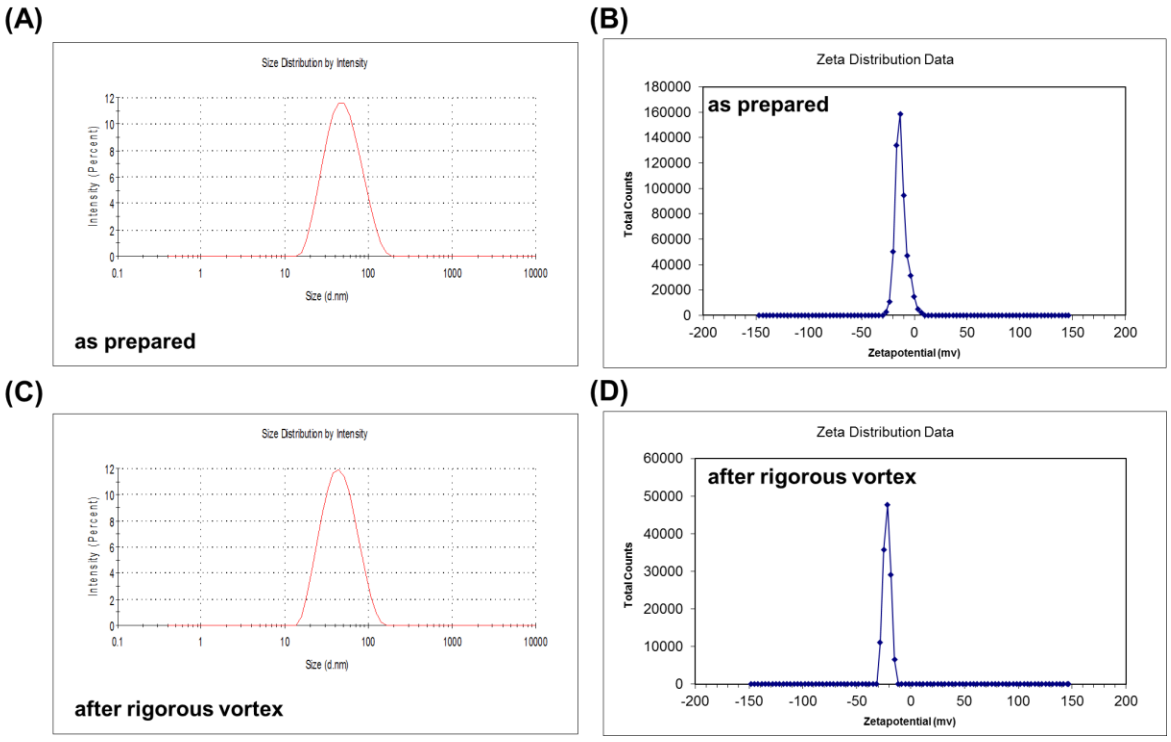

Figure S1. DLS results of (A) (C) Average diameter, 38 nm with polydispersity index (PDI) 0.15, (B) (D) Average zeta potential, −15 mV before and after rigorous vortex, respectively.

3. Electrochemistry of 2-ABP in THF Cocktail Solution.

Based on the results in cyclic voltammetry (CV) with 2-ABP in THF cocktail solution, 0.85 V vs Pt QRE has been selected to perform the following SEE measurements. Note that 0.85 V vs Pt QRE does not trigger the electropolymerization of 2-ABP, thus showing reproducible and retraceable voltammograms (red and black solid curves in Figure S2B). In contrast, as the scanned potential became more positive than 0.85 V, large hysteresis in CV was observed due to the oxidative electropolymerization of 2-ABP (Figure S2A).[S2] To simplify the electrochemical oxidation of 2-ABP during SEE measurements, the optimized potential of 0.85 V vs Pt QRE has been selected.

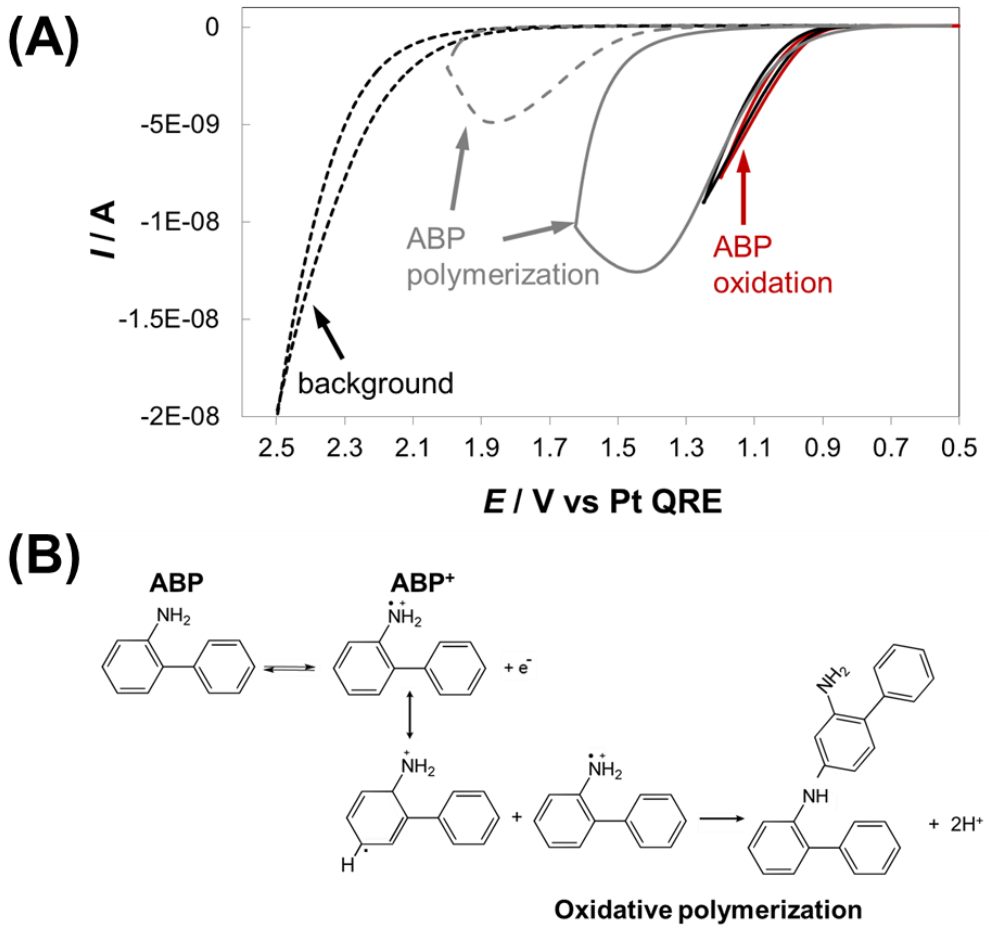

Figure S2. (A) Cyclic voltammograms of 6 mM 2-ABP in THF cocktail solutions. The scan rate was 25 mV/s. (B) A mechanistic scheme of electrochemical oxidation of 2-ABP with one electron transfer, which can further undergo electropolymerization reaction.[S2]

4. Nanopipet Voltammetry of PF_6^- Ion Transfer across the Immiscible Interface between DOS and Aqueous Buffer.

The overall charge-neutrality in NE should be acquired mainly by ingress of hydrophobic anion, PF_6^- from aqueous buffer solution to the organic phase inside a NE as reported in our previous work.[S1] During the SEE with NEs at 0.85, PF_6^- ion transfers should occur across the polarized NE interface to organic phase in NE with a diffusion control, while 2-ABP (or FcMeOH) is fully oxidized to 2-ABP^+ (or $FcMeOH^+$) until its depletion in the NE.

We applied nanopipet voltammetry to estimate the $E_{1/2}$ of PF_6^- ion transfer at a water/oil interface in lieu of NE interface, and to predict the feasibility of a coupling between ion transfer and electron transfer reactions, thereby experimentally confirming that electron transfer reactions in NEs are facilitated by ion transfer reactions. Herein, NE interface is mimicked by DOS filled nanopipet including 0.1 M tetradodecylammonium tetrakispentafluorophenyl borate in the organic phase. The nanopipet is immersed in the aqueous solution containing 1 mM NH_4PH_6 with 50 mM phosphate buffer at pH 7.5. The measured $E_{1/2}$ of PF_6^- ion transfer was –0.38 V vs Pt QRE (Figure S3), which is significantly lower than the applied potential, 0.85 V during SEE measurements. Therefore, PF_6^- ion transfer across NE interface should occur under the diffusion controlled condition, which wouldn't be a rate determining step for the oxidation of 2-ABP or FcMeOH inside NEs during SEE measurements.

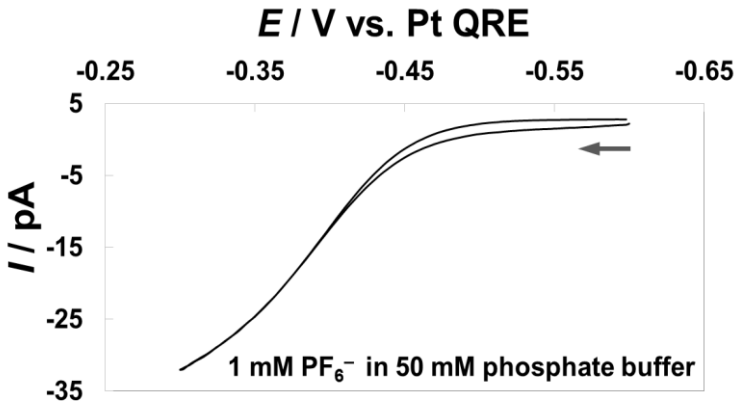

Figure S3. Nanopipet voltammogram of PF_6^- ion transfer at 120 nm diameter nanopipet filled with DOS with 0.1 M tetradodecylammonium tetrakispentafluorophenylborate. The aqueous solution contains 1 mM NH_4PH_6 in 50 mM phosphate buffer at pH 7.5. The scan rate was 25 mV/s.

5. Fitting *i-t* Decay with Bulk Electrolysis Model.

This collisional response, *i-t* decay was fitted with bulk electrolysis model as below [S3,S4]

$$i(t) = i_p e^{-\frac{mA}{V}t} \quad \text{(S1)}$$

$$m = \frac{4D_{ABP}}{\pi r_c} \quad \text{(S2)}$$

where, i_p (= 0.23 pA) is the initial peak current, t is the time (s), m is the mass-transfer coefficient, r_c (=19 pm) and A (=1.13×10^{-17} cm^2) are a contact radius and area between an UME and a NE, respectively, V (=2.87×10^{-17} cm^3 for 19 nm radius NE) is a NE volume, and D_{ABP} (=1×10^{-7} cm^2/s) is the diffusion coefficient of 2-ABP in the castor oil inside a NE determined by Stoke-Einstein equation. In Figure S3, we show a good agreement between the experimental *i-t* curve (black solid lines) and the simulation (red open circles), thus validating bulk electrolysis of 2-ABP inside a ~38 nm diameter NE.

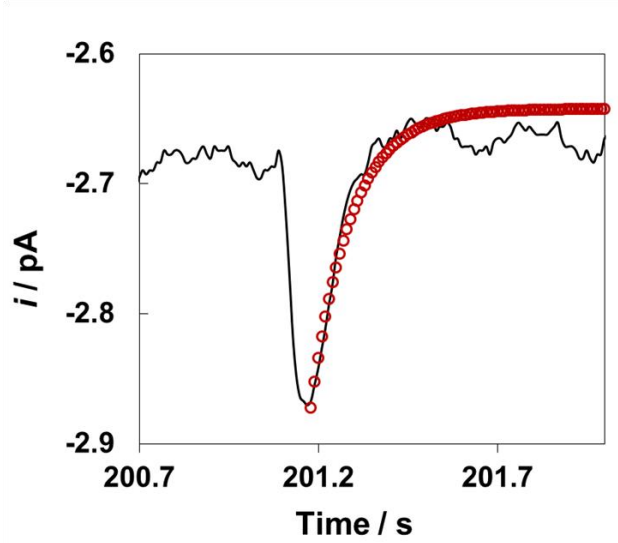

Figure S4. *i-t* curve of a 2-ABP partitioned NE colliding onto Pt UME under 0.85 V vs Pt QRE, shown in Figure 3E inset. The experimental data is fitted with simulated *i-t* behavior for the first order homogeneous electrolysis reaction shown by red open circles.

6. Additional SEE data for 2-ABP Partitioned at Intact NEs.

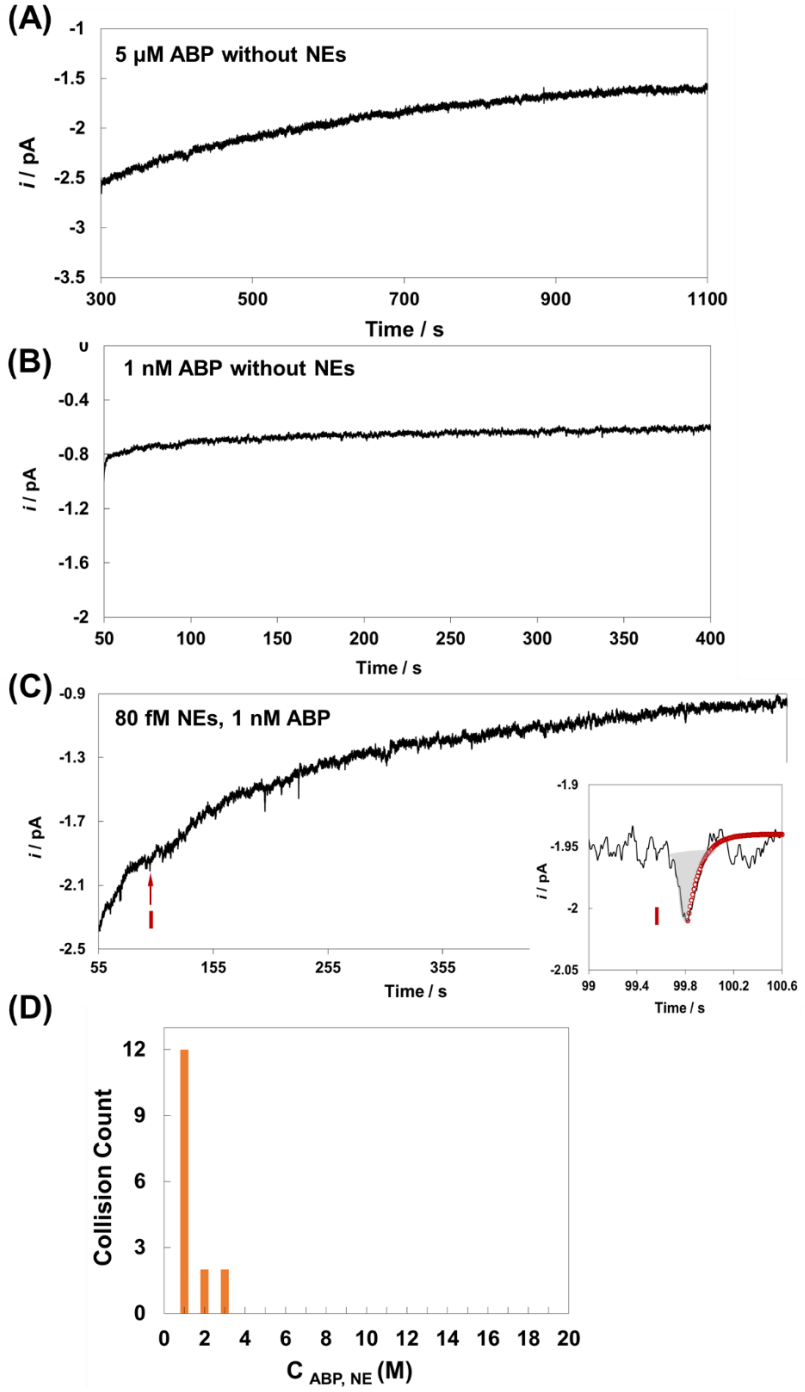

Figure S5. (A) (B) Background *i-t* curves in 5 μM ABP, 10 mM NH_4PH_6 and, 1 nM ABP, 10 mM NH_4PH_6 in the absence of NEs, respectively. (C) *i-t* curves of NE collisions at Pt UME under 0.85 V vs Pt QRE with 80 fM NEs and 1 nM 2-ABP in aqueous bulk solution. Inset shows a comparison between experimental current spike (black solid lines) and simulated one (red open circles) based on the bulk electrolysis model. (D) Concentration distribution curves of 2-ABP partitioned in NEs, $C_{ABP,\,NE}$ from the SEE data.

Additional SEE data is shown in Figure S5. In the absence of NEs, background responses with a blank sample containing either 5 μM ABP or 1 nM ABP were depicted, where c.a. 50 fA level of noise has been observed (Figure S5A and S5B). With 80 fM NEs in the aqueous solution containing 1 nM ABP, a typical *i-t* curve was observed (Figure S5B). Using the eq (1) and the charges integrated from *i-t* curve, the concentration of 2-ABP in individual NEs was estimated, and the corresponding concentration distribution curve was constructed with a $C_{ABP,\,NE}$ peaked at 1.0 M (Figure S5C). Note that the obtained current responses, i.e. the estimated $C_{ABP,\,NE}$ values (= 1.0 (± 0.9) M) are close to the limit of detection in our SEE measurements.

2-ABP	8 pM NEs	0.8 pM NEs	80 fM NEs
V_{NE} (mL)	1.607×10^{-6}	1.607×10^{-7}	1.607×10^{-8}
V_{aq} (mL)	10.00	10.00	10.00
V_{total} (mL)	$V_{aq} + V_{NE}$	$V_{aq} + V_{NE}$	$V_{aq} + V_{NE}$
slope	6.217×10^{6}	6.169×10^{7}	6.111×10^{8}
P	1.420×10^{10}	7.490×10^{9}	3.480×10^{10}

Table S1. Experimental parameters for estimating a partition coefficient, *P* of 2-ABP at various concentration of NEs.

7. SEE Data and In Situ Measurement of Partition Coefficient of FcMeOH at Intact NEs.

In order to validate our methodology for in situ measurement of partition coefficient at the intact NEs, we performed SEE measurements with other compounds exhibiting aromatic property, i.e., FcMeOH. As we did for 2-ABP, we performed SEE at a constant potential 0.40 V vs. QRE under three different concentrations of NEs such as 8 pM, 0.8 pM, and 80 fM in the presence of 1 nM ~ 10 μM of FcMeOH in the aqueous buffer solution.

In Figure S6, the resulting *i-t* responses during SEE measurements are depicted. Each characteristic current spike appears with showing well-defined behavior of bulk electrolysis model, thus implying the partitioning of FcMeOH inside NEs (Insets in Figure S6). The integration of a current spike over time gives charges needed for electrolysis of FcMeOH, thus an amount of FcMeOH

partitioned in a NE. Using eq (1), the overall distribution of C_{FcMeOH}^{NE} estimated from current spikes, is illustrated in Figure S6B, S6D, and S6F. The resultant C_{FcMeOH}^{NE} ranges 14.0 ~ 17.0 M with a peak at 15.5 M as observed with 2-ABP, which is also consistent with the maximum capacity of given NEs, 15.8 M for ferrocene determined by our previous work.[S1] Notably, a narrow distribution of C_{FcMeOH}^{NE} was observed, which could be attributed to the fully equilibrated system as well as monodisperse NEs.

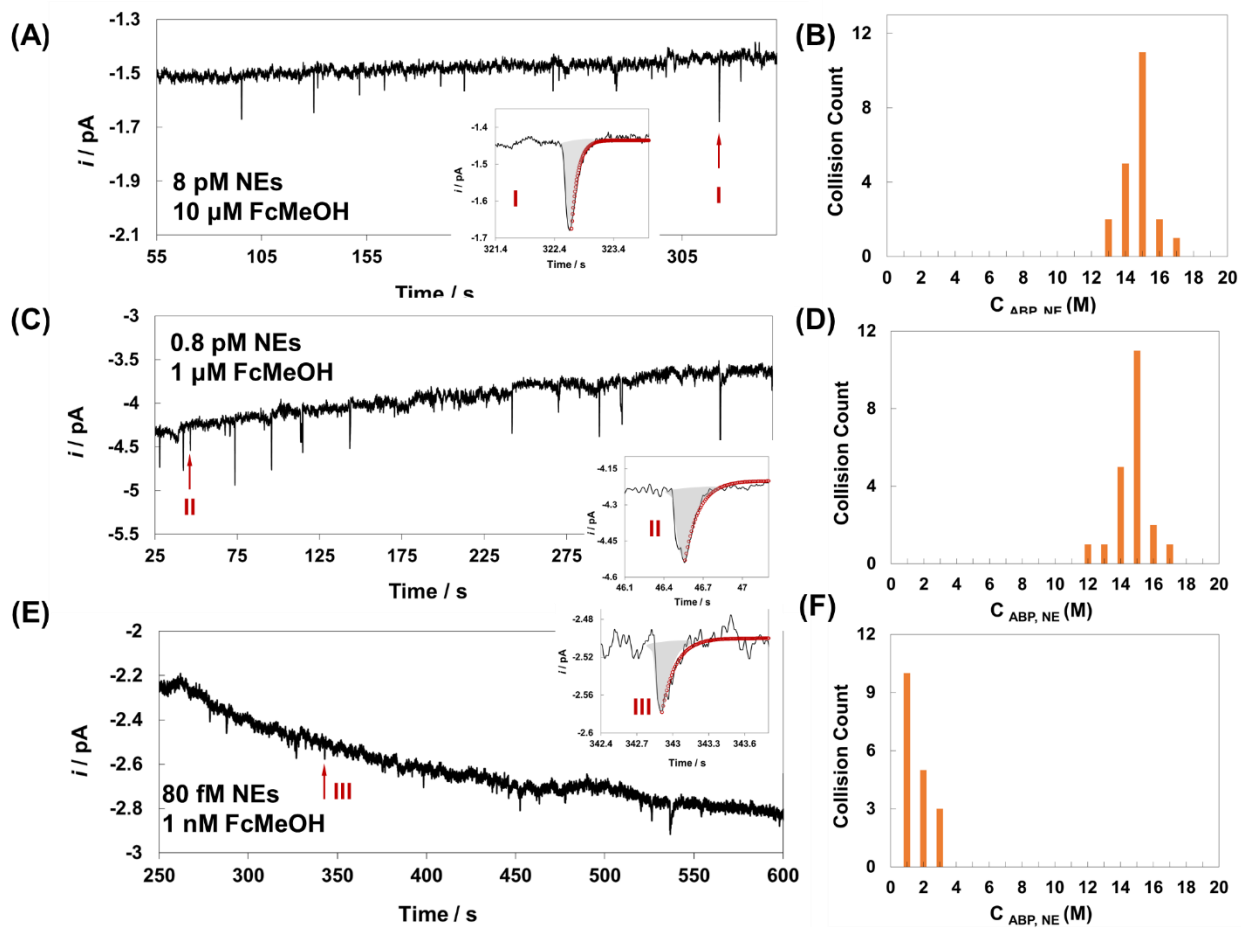

Figure S6. (A),(C), (E) *i-t* curves of NE collisions at Pt UME under 0.40 V vs Pt QRE with (8 pM NEs + 10 μM FcMeOH), (0.8 pM NEs + 1 μM FcMeOH), and (80 fM NEs + 1 nM FcMeOH), respectively. Each inset shows a comparison between experimental current spike (black solid lines) and simulated one (red open circles) based on the bulk electrolysis model. (B), (D), (F) Concentration distribution curves of FcMeOH partitioned in NEs, $\boldsymbol{C_{FcMeOH}^{NE}}$ from the corresponding SEE data.

We also constructed a plot of C_{FcMeOH}^{NE} vs. total concentration of FcMeOH, C_{FcMeOH}^{tot} by combining all the average peak values of C_{FcMeOH}^{NE} in SEE data in the presence of 8 pM, 0.8 pM, 80 fM NEs (Figure S7). Three linear curves were obtained with respectively different slopes (determined by the least square regression).

Here, we applied the same formulation for the relationship between C_{FcMeOH}^{NE} and C_{FcMeOH}^{tot} as shown in eq (2) ~ eq (5). Finally, an implicit equation relating C_{FcMeOH}^{NE} with C_{FcMeOH}^{tot} is obtained as below,

$$C_{FcMeOH}^{NE} = \left[\frac{V_{total}}{\frac{V_{aq}}{P}+V_{NE}}\right] \cdot C_{FcMeOH}^{tot} \qquad \text{(S3)}$$

This relationship, eq (S3) is readily used to extract the partition coefficient, *P* with experimentally estimated C_{FcMeOH}^{NE} from the readout of SEE measurements under a series of various C_{FcMeOH}^{tot}. Using three slopes in Figure S7, the respective experimental values (i.e. V_{total}, V_{aq}, and V_{NE}), and eq (S1), the apparent partition coefficient, *P* could be determined as 2.6 (± 1.6) × 10^9. This determined *P* by SEE measurements is also ~ 7 orders of magnitude higher than the reported partition coefficient of FcMeOH between two phase, 1,2–dichlorobenzene and water (*P* = 82) (or, *K* in eq (9)).[S5] This result is consistent with 2-ABP, which could be attributed to the intermolecular interaction between π* of aromatic ring and the lone pair in DOS as well as hydrogen bonding inside NEs as well. In Figure S8, we depicted the optimized geometry of FcMeOH–DOS inside NEs determined by the molecular dynamics simulation.

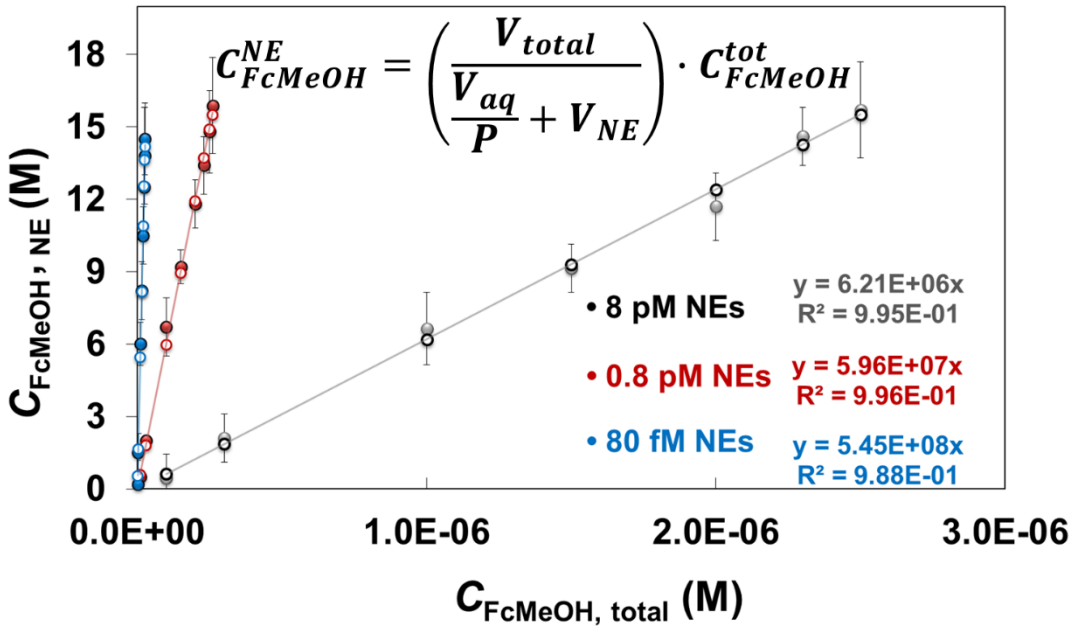

Figure S7. A plot of C^{NE}_{FcMeOH} vs. C^{total}_{FcMeOH} in the presence of various concentration of NEs, 8 pM (black closed circles), 0.8 pM (red closed circles), and 80 fM (blue closed circles). The respective slopes and squared correlation coefficients, R^2 from the least square regression are shown in the bottom right. Each error bar represents the standard deviation from 1500~2000 current spikes observed in SEE measurements under the each given condition.

FcMeOH	8 pM NEs	0.8 pM NEs	80 fM NEs
V_{NE} (mL)	1.607×10^{-6}	1.607×10^{-7}	1.607×10^{-8}
V_{aq} (mL)	10.00	10.00	10.00
V_{total} (mL)	$V_{aq} + V_{NE}$	$V_{aq} + V_{NE}$	$V_{aq} + V_{NE}$
slope	6.208×10^{6}	5.959×10^{7}	5.454×10^{8}
P	1.91×10^{9}	1.42×10^{9}	4.40×10^{9}

Table S2. Experimental parameters for estimating a partition coefficient, P of FcMeOH at various concentration of NEs.

8. Molecular Dynamics Simulation Results

Quantum chemistry calculations were carried out using Spartan (Wavefunction Inc., Irvine, California, USA, 2014, 1.1.8 version). The molecules of 2-ABP (2-Aminobiphenyl) or FcMeOH

(ferrocene methanol), and DOS (bis(2-ethylhexyl)- sebacate) were built, and combinations of DOS molecules with 2-ABP molecules or FcMeOH molecule (model 1, 2, 3, and 4 in Table S3) systems were geometrically equilibrated. Conformer distribution for geometrically equilibrated model 1, 2, 3, and 4 was found using Molecular Mechanics, Merck Molecular Force Field (MMFF) calculation method. The most stable 100 structures were stabilized under Semi Empirical, PM3 method to find the most stable 20 structures with the least energy values.

Thermodynamic parameters for DOS, 2-ABP, FcMeOH, model 1, 2, 3, and 4 structures were implemented with Hartree-Fock method, and all basis sets and preceding calculations were done with the Slater type functions applied in the Spartan program for both geometry optimization and thermodynamic energy values.

Molecule	$G°$/ kJ/mol	$\Delta G°$/ kJ/mol	$\beta \quad (\exp(-\Delta G^0 / RT))$
2-ABP	-1.336×10^6		
DOS	-3.403×10^6		
FcMeOH	-4.571×10^6		
model 1 (one 2-ABP + one DOS)	-4.739×10^6	-11.70	1.12×10^2
model 2 (one 2-ABP + three DOS)	-1.155×10^7	-7026	*
model 3 (two 2-ABP + three DOS)	-1.289×10^7	-7555	*
model 4 (one FcMeOH + one DOS)	-7.976×10^6	-1946	*

Table S3. Calculated energies for models with 2-ABP, FcMeOH and DOS molecules (*: too large to be defined).

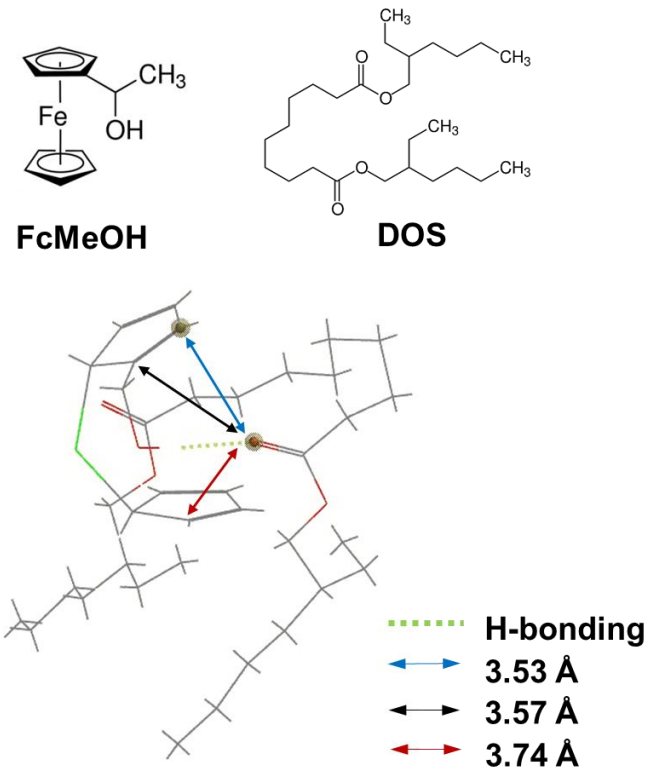

Figure S8. Geometry optimized structure of FcMeOH with DOS molecule. The interaction between lone pair from oxygen of DOS and π system of aromatic ring in FcMeOH (red, blue and black arrows) as well as hydrogen bonding (green dotted line) has been depicted.

References

S1. Sabaragamuwe, S. G.; Conti, D.; Puri, S. R.; Andreu, I.; Kim, J, Single-Entity Electrochemistry of Nanoemulsions: The Nanostructrual Effect on Its Electrochemical Behavior, *Anal. Chem.*, **2019**, 91, 9599-9607.

S2 . Badawy, W. A.; Ismail, K. M.; Khalifa, Z. M.; Medany, S. S., Poly(2-aminobiphenyl), Preparation, Characterization, Mechanism, and Kinetics of the Electropolymerization Process, *J. Appl. Polym. Sci.*, **2012**, 125, 3410-3418.

S3 . Kim, B. K.; Boika, A.; Kim, J.; Dick, J. E.; Bard, A. J., "Characterizing Emulsions by Observation of Single Droplet Collisions- Attoliter Electrochemical Reactors", *J. Am. Chem. Soc.*, **2014**, 136, 4849-4852.

S4. Bard, A. J.; Faulkner, L. R., "Electrochemical Methods: Fundamental and Applications", **2004**, 2nd Ed., John Wiley & Sons INC.

S5. Peljo, P.; Qiao, L.; Murtomäki, L.; Johans, C.; Girault, H. H.; Kontturi, K., Electrochemically Controlled Proton-Transfer-Catalyzed Reactions at Liquid-Liquid Interfaces: Nucleophilic Substitution on Ferrocene Methanol, *Chem. Phys. Chem*., **2013**, 14, 311-314.